



# Micro and nano sized particles in leachates from agricultural soils: Phosphorus and sulfur speciation by X-ray micro-spectroscopy

Gbotemi A. Adediran<sup>a,\*</sup>, Daniel Lundberg<sup>b</sup>, Gunnar Almkvist<sup>b</sup>, Ana E. Pradas del Real<sup>c,1</sup>, Wantana Klysubun<sup>d</sup>, Stephen Hillier<sup>a,e</sup>, Jon Petter Gustafsson<sup>a</sup>, Magnus Simonsson<sup>a,\*</sup>

<sup>a</sup> Department of Soil and Environment, Swedish University of Agricultural Sciences, Box 7014, Uppsala 750 07, Sweden

<sup>b</sup> Department of Molecular Sciences, Swedish University of Agricultural Sciences, Box 7015, Uppsala 750 07, Sweden

<sup>c</sup> ESRF–The European Synchrotron, 1D21, 71 Avenue des Martyrs, Grenoble 38000, France

<sup>d</sup> Synchrotron Light Research Institute, 111 Moo 6, Suranaree, Muang, Nakhon Ratchasima, Thailand

<sup>e</sup> The James Hutton Institute, Craigiebuckler, Aberdeen AB15 8QH, United Kingdom

## ARTICLE INFO

### Article history:

Received 24 August 2020

Revised 28 October 2020

Accepted 30 October 2020

Available online 30 October 2020

### Keywords:

Leachates

Colloids

Nanoparticles

Phosphorus

Sulfur

Speciation

## ABSTRACT

Colloids and nanoparticles leached from agricultural land are major carriers of potentially bioavailable nutrients with high mobility in the environment. Despite significant research efforts, accurate knowledge of macronutrients in colloids and nanoparticles is limited. We used multi-elemental synchrotron X-ray fluorescence (XRF) microscopy with multivariate spatial analysis and X-ray atomic absorption near-edge structure (XANES) spectroscopy at the P and S K-edges, to study the speciation of P and S in two fractions of leached particles, >0.45 and <0.45  $\mu\text{m}$  respectively, collected from four tile-drained agricultural sites in Sweden. P K-edge XANES showed that organic P, followed by P adsorbed to surfaces of aluminum-bearing particles were the most common forms of leached P. Iron-bound P (Fe-P) forms were generally less abundant (0–30 % of the total P). S K-edge XANES showed that S was predominantly organic, and a relatively high abundance of reduced S species suggests that redox conditions were adverse to the persistence of P bound to Fe-bearing colloids in the leachates. Acid ammonium-oxalate extractions suggested that P associated with Al and Fe (Al-P and Fe-P) in most cases could be explained by the adsorption capacity of non-crystalline (oxalate-extractable) oxides of Al and Fe. These results improve our understanding of particulate P and S speciation in the vadose zone and helps in developing effective technologies for mitigating colloidal driven eutrophication of water bodies near agricultural land.

© 2020 The Author(s). Published by Elsevier Ltd.

This is an open access article under the CC BY license (<http://creativecommons.org/licenses/by/4.0/>)

## 1. Introduction

Diffuse loss of macronutrients from agricultural land remains one of the main drivers of eutrophication, leading to harmful algae bloom, deterioration of drinking water quality, and loss of biodiversity in affected aquatic systems (Zou et al., 2020). The eutrophication of surface and subsurface waters depends on nutrient concentration as well as molecular speciation (Liu et al., 2014; Read et al., 2014). It has been shown that most elements mobilized from soils are associated with colloidal and nanoparticulate phases (Gottselig et al., 2017a; Gottselig et al., 2014; Hill and Aplin, 2001; Jarvie et al., 2012). Knowledge of their speciation and potential

bioavailability is critical in order to reduce the loss of nutrients from agricultural lands and to predict environmental risks.

Colloids and nanoparticles are small enough to withstand gravitational settling. They consist of mineral particles, detrital organic matter and living bacterial cells (Gustafsson and Gschwend, 1997). Due to their large specific surface area and high reactivity, clay minerals including Fe/Al hydroxides (< 2  $\mu\text{m}$ ) and particulate organic matter are considered as the most mobile components of the soil system and as important vehicles of nutrient transport from the soil profile (Das et al., 2019; Regelink et al., 2013). Natural colloids like iron (Fe) and aluminum (Al) oxides, silica and organic molecules in natural aquatic systems have been linked to weathering and mineralization processes in the soil (Holtzman and Lehman, 1998; Tsao et al., 2011). However, the knowledge of the nature and properties of macronutrients in colloids and nanoparticles mobilized from agricultural land is limited. One of the reasons for this is the adherence to operational definitions of 'dissolved'

\* Corresponding authors.

E-mail addresses: [gbotemi.adediran@slu.se](mailto:gbotemi.adediran@slu.se) (G.A. Adediran), [magnus.simonsson@slu.se](mailto:magnus.simonsson@slu.se) (M. Simonsson).

<sup>1</sup> Present address: Madrid Institute for Agricultural Research (IMIDRA), N-II km 38,200, 28800 Alcala de Henares, Spain.

compounds based solely on filtration through a filter; e.g., of 0.45- $\mu\text{m}$  pore size (Hall et al., 1996; Heathwaite et al., 2005). However, the filtrate is likely to include fine nanoparticles as well as dissolved species (Gimbert et al., 2007).

Surface runoff, subsurface lateral flow and vertical percolation (leaching) are the major hydrological pathways through which soil nutrients are transported. In many agricultural systems, especially under high-intensity rainfall events, surface runoff is the main route of nutrient loss from the soil (Ma et al., 2016; Sharpley et al., 1993). However, transport by rapid vertical flow in macropores can be the predominant pathway in flat areas, and this is considered as the main pathway of nutrient loss in central Sweden (Andersson et al., 2013; Ulén and Snäll, 2007). Of all nutrients, the loss of phosphorus (P) from arable land is of strategic importance to the Swedish environment, especially the eutrophication of the Baltic Sea, one of the largest brackish water areas in the world (Eriksson et al., 2013; Murray et al., 2019). A similar scenario of P-driven eutrophication is applicable in other parts of Europe (Ulén et al., 2007) and North America (Council, 2011; Kleinman et al., 2019). Moreover, successive P inputs over time have resulted in a build-up of P in many soils globally (Liu et al., 2015). This accumulated 'legacy P' is characterized by slow remobilization in agricultural soils, acting as a continuous source of P pollution in aquatic environments (Bergström et al., 2015; Sharpley et al., 2013).

According to prior studies, colloidal and nanoparticulate P may constitute up to 80 % of total P in leachates from agricultural land (Gottselig et al., 2014; Liu et al., 2014; Sharma et al., 2017). Elucidating the chemical speciation of this P is critical to unravel the processes that govern particulate P retention and desorption in soils, and to predict particulate P reactivity in the receiving environments. For example, the P that exists as iron phosphate or is bound to the surfaces of iron-bearing minerals, like ferrihydrite or goethite, would be more sensitive to redox conditions (Henderson et al., 2012; Murray and Hesterberg, 2006). On the other hand, the P that exists as aluminum phosphate or is bound to the surfaces of aluminum oxide/hydroxide particles, as well as P that exists as hydroxyapatite or other calcium phosphates, would be more vulnerable to changes in pH conditions (Guidry and Mackenzie, 2003). Organic P, on the other hand, would be susceptible to microbial mineralization and biotransformation (Prentice et al., 2019).

There have been few attempts at deciphering the speciation of P in suspended particles leached from arable soils under field conditions. A study on colloids that were artificially detached from the soils by mechanical dispersion, showed colloidal P to be mainly inorganic, with P associated with Fe- and Al minerals as the main species (70–83 %) followed by hydroxyapatite (17–20 %) (Liu et al., 2014). The capacity of mineral surfaces to adsorb phosphate varies greatly depending on pH and the crystallinity of the oxide phase. The absence of a sharp boundary between surface adsorption and formation of a separate phosphate phase through precipitation further complicates the assessment of maximum adsorption capacity (Hesterberg, 2010; Van Riemsdijk and Lyklema, 1980). Notwithstanding, the maximum sorption is reported to be modest on phyllosilicate clays, with values ranging from 8 to 13 mmol  $\text{kg}^{-1}$  for 2:1 minerals (Violante and Pigna, 2002) and up to 42 in 1:1 minerals (Gray-Wannell et al., 2020); it is roughly one or two orders of magnitude greater in allophane, crystalline gibbsite and goethite (Khare et al., 2005; Violante and Pigna, 2002), and approximately 1700 and 3300 mmol  $\text{kg}^{-1}$  in ferrihydrite and amorphous  $\text{Al}(\text{OH})_3$ , respectively (Hesterberg, 2010; Khare et al., 2005).

Sulfur (S) is an essential macronutrient used by plants in amounts similar to those of P (Kopriva et al., 2019). The majority of S transported to aquatic environments comes from soils and wetlands, and the S is mostly released in organic forms

(Fakhraee et al., 2017). Organic S in soils exists in reduced species (sulfides, thiols), intermediately oxidized species (sulfoxides, sulfones and sulfonates) and fully oxidized S in sulfate esters. In a study of S in two Swedish agricultural soils, sulfate esters were the single most abundant category, representing 40–64 % of the S, whereas inorganic sulfate was less than 2 % (Boye et al., 2011). However, the redox state of organic S may depend on the redox conditions of the soil, with more abundant reduced species and less intermediate and oxidized species in waterlogged soils, and vice versa (Prietz et al., 2009b). Most importantly, increases in P eutrophication have been linked to S biotransformation and mineralization during the breakdown of organic matter (Lamers et al., 2002; van Diggelen et al., 2014). Therefore, the speciation of S in colloids leached from the soil carries information on processes relevant for both S itself and for P.

To our knowledge, there is no study that has examined the molecular speciation of P and S simultaneously in colloids and nanoparticles leached from agricultural land under natural conditions. The aim of this study was to reveal the molecular speciation of these elements in two fractions of naturally leached particles,  $>0.45$  and  $<0.45$   $\mu\text{m}$ , respectively, by using synchrotron X-ray fluorescence microscopy and X-ray absorption near-edge structure (XANES) spectroscopy.

## 2. Methodology

### 2.1. Study sites

Leachates from tile-drained fields at four agricultural sites situated in the drainage basin of the North Sea, the Baltic Sea and Vänern, the largest lake in the European Union, were selected for this study. The sites include three clayey soils, Krusenberg (59°14' N, 17°41' E), Lilla Böslid (56°35' N, 12°56' E) and Lanna (58°21' N, 13°07' E), as well as a sandy soil, Mellby (56°29' N, 12°59' E). The trials are equipped with plots that are individually tile-drained at 0.9–1.0 m depth and have an area of 42  $\text{m}^2$  at Krusenberg, 320–1700  $\text{m}^2$  at the other sites. Flow-proportional bulk samples are collected in a drain station over 14 consecutive days from each plot. The trials receive 8–20  $\text{kg ha}^{-1}$  of P annually, supplied as mineral fertilizer at Lanna and Lilla Böslid, and cattle- and pig slurry at Krusenberg and Mellby, respectively. A detailed description of the sites is presented in the supplementary material (S1).

### 2.2. Chemical analyses

Bulk leachates were analyzed for pH, alkalinity and electric conductivity (EC); ionic strength was calculated from the latter with the Marion–Babcock equation. Total organic carbon (TOC) and total nitrogen were measured in unfiltered samples by combustion and catalytic oxidation, respectively (Shimadzu TOC-VCPH). Suspended materials were collected on a 0.2- $\mu\text{m}$  membrane filter and weighed. Three operational P fractions were analyzed: (1) Total P by flow analysis of molybdate-reactive phosphate (Technicon Autoanalyzer 3) after oxidation of non-filtered samples with peroxodisulfate (ISO-6878, 2004); (2) total P  $<0.2$   $\mu\text{m}$  after filtration, using the same digestion and analysis as for the total P; (3) molybdate-reactive (ortho)phosphate (ISO-15923-1:2013 2013) after filtration ( $<0.2$   $\mu\text{m}$ ). The difference (1) – (2) will be referred to as 'particulate P  $>0.2$   $\mu\text{m}$ '; (2) – (3) is 'non-orthophosphate P  $<0.2$   $\mu\text{m}$ '.

### 2.3. Isolation of leached particles

Leachate particles were isolated in two steps: First, particles  $>0.45$   $\mu\text{m}$  were collected on a 0.45- $\mu\text{m}$  (Durapore® Membrane) filter. Second, particles in leachates from the first step were collected

on a 10 kDa (Ultracel® Membrane) filter to yield a size range from 10 kDa to 0.45  $\mu\text{m}$ . These fractions are henceforth referred to as 'coarse particles' ( $>0.45 \mu\text{m}$ ) and 'fine particles' ( $<0.45 \mu\text{m}$ ), respectively.

The isolated particles were rinsed twice with Milli-Q water and freeze-dried for bulk-chemical analysis, or stored wet at 5°C until further analysis as specified in Table S1. The freeze-dried particles were analyzed for bulk chemistry after digestion in a mixture of  $\text{HNO}_3$ ,  $\text{HCl}$  and  $\text{HF}$  according to SFS-EN13656 (2002). Non-crystalline and organically-bound metals were extracted with 0.2-M ammonium oxalate at pH 3 in darkness (Jiang et al., 2015). Elements in bulk digests and oxalate extracts were analyzed by ICP-SFMS (Church et al., 2017). Oxalate-extractable Al, Si, Fe, P and S were divided by the respective bulk concentration to yield a weight percent representing the 'extractability' in oxalate.

#### 2.4. Mineralogical analysis by X-ray diffraction (XRD)

Coarse particles in one leachate from each plot were isolated on a 0.45- $\mu\text{m}$  silver-filter membrane (Millipore AG4502550) and scanned using copper  $K\alpha$  radiation from 3 to 45°  $2\theta$  in (i) air-dried state, (ii) after glycolation, and (iii) after heating to 300°C for one hour. Clay minerals were semi-quantified using a Reference-Intensity Ratio factor approach (Hillier, 2003). A 'C/QF' ratio, crudely estimating the relative proportions of phyllosilicates to non-clay minerals, the latter principally consisting of quartz and feldspars, was also calculated from the peak heights of the phyllosilicate peak near 5 Å and the quartz-K-feldspar doublet at about 4.26 Å in the diffractogram obtained after heating. The 5 Å peak was chosen because of its proximity to the 4.26 Å doublet which means any sample related errors will be near constant for the two peaks, and because the 5 Å peak in the heated sample, as 002 of the peak near 10 Å (little intensity remained in the  $>10 \text{Å}$  range following heating) represents most of the clay minerals present.

#### 2.5. Bulk P K-edge XANES

P K-edge XANES spectra were collected from freeze-dried particle fractions at beam line 8 of the Synchrotron Light Research Institute (SLRI) in Nakhon Ratchasima, Thailand (Klysubun et al., 2020); the analysis is henceforth referred to as 'bulk XANES' as distinct from spot-wise ' $\mu$ -XANES' described below. The beamline was equipped with an InSb (111) crystal monochromator and a solid-state 13-element Ge fluorescence detector. The beamline has a photon flux that ranges from  $4 \times 10^7$  to  $3 \times 10^{11}$  photons  $\text{s}^{-1}$  (100 mA) $^{-1}$ , and a high energy resolution of  $4.6 \times 10^{-4}$  at 3206 eV and  $3.8 \times 10^{-4}$  at 6539 eV (Klysubun et al., 2020). The beam size was  $18 \times 2 \text{mm}$  and the beam flux was  $2 \times 10^{11}$  photons  $\text{s}^{-1}$  (100 mA) $^{-1}$ . The particles were homogenized and mounted on P-free Kapton tape. To minimize X-ray absorption by air, the sample compartment was filled with helium gas. Spectra of samples and reference P-compounds were recorded over 2100–2320 eV. The step size was 2 eV at 2100–2132 eV; 1 eV at 2132–2144 eV; 0.2 eV at 2144–2153 eV; 0.3 eV at 2153–2182 eV; and 5 eV at 2182–2320 eV. The dwell time was 3 s per energy step during all measurements.

#### 2.6. Synchrotron micro-focused XRF and XANES

Micro-focused XRF imaging and micro-focused XANES analysis (referred to as ' $\mu$ -XRF' and ' $\mu$ -XANES' in the following) was performed at the X-ray microscopy beamline ID21 of the European Synchrotron Research Facility (ESRF), France. The beamline is optimized for micro-spectroscopy with submicron resolution in the 2 to 9.5 keV energy range allowing the mapping and XANES analysis of both low and high energy elements (Salomé et al., 2013). Samples (Table S1) were first mixed with a vortex mixer, deposited on

Ultralene® thin film, and allowed to dry at 25 °C. The detectors on the beamline includes a  $\text{Si}_3\text{N}_4$  diode for  $I_0$  and a silicon drift detector (SGS Sensortech 80  $\text{mm}^2$  active area) for the emitted X-ray fluorescence. Focusing of the X-ray beam ( $0.5 \times 1.2 \mu\text{m}$ ) was performed by a Kirkpatrick-Baez mirrors system. A double beam set-up was used by selecting both the first and the third harmonic in order to allow the simultaneous mapping of low- and high-Z elements. The photon flux was  $1.9739 \times 10^9$  photons  $\text{s}^{-1}$  at 2.5 keV. High-resolution  $\mu$ -XRF images of elements were acquired with a dwell time of 100 ms using a step size of  $1.0 \times 1.0 \mu\text{m}^2$  for the coarse particles and  $0.5 \times 0.5 \mu\text{m}^2$  for the fine particles.

Spot-wise  $\mu$ -XANES of P and S was performed at spots with varying concentration according to the elemental imaging. P and S K-edge  $\mu$ -XANES spectra were recorded in fluorescence mode by single-point acquisition over 2.10–2.22 and 2.45–2.55 keV energy ranges for P and S respectively, with 0.2 eV steps using the moving (Si 111) monochromator of ID21. For both measurements, the calibration of the monochromator energy was done using hydroxypapatite for P and L-cysteine for S. At every selected spot, 8 to 12  $\mu$ -XANES scans were collected. Collected  $\mu$ -XANES spectra were examined for possible beam damage and up to 6 high-quality spectra were selected and merged to represent a spot.

#### 2.7. Analysis of X-ray fluorescence data

The  $\mu$ -XRF spectra were dead-time corrected and normalized to incoming beam intensities before deconvolution. High-resolution elemental images were obtained after fitting each pixel spectrum using the PyMca X-ray Fluorescence Toolkit (Solé et al., 2007). The spatial correlation of P with relevant elements (S, Al, Ca and Fe) is shown using 3-colour 'RGB' (red-green-blue) correlator. Principal-component analysis (PCA) of deconvoluted elemental intensities of Mg, Al, Si, P, S, K, Ca and Fe was performed using JMP® Pro 14; mean centering of each element and scaling to unit standard deviation was part of the procedure.

#### 2.8. Analysis of XANES data

The P speciation by both  $\mu$ -XANES and bulk XANES was estimated by linear-combination fitting (LCF) (Tannazi and Bunker, 2005). Because P in soils, sediments and particles is most often associated with Al, Ca, Fe and organic matter (Adediran et al., 2020; Werner and Prietzel, 2015), 12 standard P spectra (Fig. S1) were selected from a large library of model precipitates and sorption species of P with these elements and materials (Gustafsson et al., 2020). In the following, Ca phosphates will be referred to as 'Ca-P' and were fitted with spectra of apatite (from Taiba, Sudan), amorphous calcium phosphate, and/or hydroxypapatite. Precipitates and sorption species of P with (hydrated) oxides of Al and Fe will be denoted 'Al-P' and 'Fe-P', respectively. The former category was fitted with spectra of aluminum phosphate, P adsorbed to amorphous aluminum hydroxide, gibbsite, and/or allophane; the latter with spectra of iron phosphate, P adsorbed to ferrihydrite and/or goethite. Phosphate in organic matter will be called 'org-P', fitted with phytate (inositol hexakisphosphate) and/or natural soil organic phosphorus from forest mor (SOP). A detailed description of the standard compounds is available in Gustafsson et al. (2020).

The LCF was performed on normalized spectra using the Demeter Athena software (Ravel and Newville, 2005). No energy shifts were permitted, and the component sum was not forced to 100 %. A maximum of 4 of the 12 reference compounds were allowed. A least-squares algorithm from 2144.05 to 2184.05 eV was used. The goodness of the fit was estimated by calculating the residual  $R$  factor of the fit:  $R = \sum_i (\text{experimental}_i - \text{fit}_i)^2 / \sum_i (\text{experimental}_i)^2$ ,

**Table 1**

Site-average texture and soil organic carbon, leachate concentrations, annual leaching of particulate and dissolved organic matter (estimated as  $2 \times$  total organic carbon, TOC), suspended solids  $>0.2 \mu\text{m}$ , total phosphorus, P in particles  $>0.2 \mu\text{m}$ , P in particles  $<0.2 \mu\text{m}$ , orthophosphate (molybdate-reactive  $\text{PO}_4\text{-P}$  after filtration to  $<0.2 \mu\text{m}$ ).

Variable	Krusenberg	Lilla Böslid	Lanna	Mellby
<i>Properties of topsoil (0–30 cm)</i>				
Texture class	clay loam	clay loam	silty clay	loamy sand
Percent clay	32	30	45	8.0
Percent organic C	1.2	1.9	1.9	3.3
<i>Properties of subsoil (30–100 cm)</i>				
Texture class	clay	silty clay loam	clay	loamy sand
Percent clay	58	40	60	5.9
<i>Leachate concentrations</i>				
pH	7.4	7.7	7.5	6.8
Alkalinity ( $\text{meq l}^{-1}$ )	1.3	4.3	3.7	1.2
Electric conductivity ( $\text{mS m}^{-1}$ )	20	58	39	37
Ionic strength ( $\text{mmol l}^{-1}$ )	2.9	8.3	5.6	5.3
<i>Annual leaching (<math>\text{kg ha}^{-1} \text{yr}^{-1}</math>)</i>				
Suspended solids $>0.2 \mu\text{m}$	4 000	270	410	15
$2 \times$ TOC	160	44	30	84
Total P	5.6	0.46	0.46	0.15
Particulate P $>0.2 \mu\text{m}$	5.1	0.39	0.43	0.08
Non-orthophosphate P $<0.2 \mu\text{m}$	0.09	0.01	0.01	0.00
Orthophosphate-P	0.40	0.06	0.02	0.07

where experimental<sub>i</sub> and fit<sub>i</sub> represent observed and fitted intensity at the *i*th energy step, respectively; the sums ( $\Sigma$ ) are over 142 data points as flattened mu ( $E$ ). The lower the *R* factor, the better the fit. The differences between the *R* factor of the best ten LCF combinations was less than 10%. The means and the standard deviation of the best 10 combinations were calculated and reported.

To resolve the S species in the leached particles, internally calibrated spectra of 19 model compounds (Table S2) were used to fit the normalized S *K*-edge XANES spectra using the LINEST function in Microsoft® Excel (Almkvist et al., 2010). In this, a least squares method was used to optimize a fit to the experimental data, using up to 15 reference spectra simultaneously. This approach allows more accurate partitioning of organic sulfate esters from inorganic sulfate, a differentiation that is not possible by traditional Gaussian-curve fitting (Prietz et al., 2011). The fitted S species were grouped into reduced (peak energy  $<2475$  eV), intermediate (2475–2479 eV) and highly oxidized S forms ( $>2479$  eV). Unlike in P, spot-wise variation in S speciation was not investigated, as high-quality S *K*-edge XANES fits were obtained only after merging all spectra from all spots into one spectrum per sample.

### 3. Results

#### 3.1. Chemical and mineralogical composition of leached particles

The soil texture at the study sites ranged from loamy sand to clay. The organic-C content of the topsoil was 1–2 % at the three clayey sites, and 3 % in the loamy sand of Mellby (Table 1). During the study period (May 2017 to April 2019) leachates, on average for each site, had near-neutral pH with alkalinity that ranged from 1 to 4  $\text{mmolc l}^{-1}$  and electric conductivity from 20 to 58  $\text{mS m}^{-1}$  (Table 1). The annual leaching of suspended materials ( $>0.2 \mu\text{m}$ ) was several hundred  $\text{kg ha}^{-1}$  on an annual basis at Lilla Böslid and Lanna, exceptionally high from individual plots at Krusenberg (range 380–7800  $\text{kg ha}^{-1} \text{yr}^{-1}$ ) potentially due to the small plot size and lateral flow from the surroundings at this site, and more than an order of magnitude less at Mellby. TOC was analyzed in unfiltered leachates and consists of both dissolved and particulate organic matter. Leaching of organic matter ( $\text{kg ha}^{-1} \text{yr}^{-1}$ ), estimated as  $2 \times$  TOC, corresponded to 4–17 % of the suspended materials ( $>0.2 \mu\text{m}$ ) at the clayey sites, and exceeded it six fold at Mellby, indicating that TOC was to a great extent dissolved or finer

than  $0.2 \mu\text{m}$  at least at the latter site. At the clayey sites, particle-bound P ( $>0.2 \mu\text{m}$ ) represented the vast majority of the leached P, whereas orthophosphate was an important constituent at Mellby.

The coarse particles were generally of clay size (approximately  $2 \mu\text{m}$  or less). They had  $\text{SiO}_2$  and  $\text{Al}_2\text{O}_3$  approximately at a 2:1 mass ratio (Table 2), which is intermediary to (Al-rich) dioctahedral clay minerals on the one hand, and trioctahedral clay, quartz and K-feldspar on the other. PCA demonstrated strong spatial correlation of Al and Mg, suggesting the presence of partly trioctahedral clay minerals (Figs. 1–3a). With the exception of Mellby, where particles  $>0.45 \mu\text{m}$  were too scarce to permit isolation for XRD, the mineralogical analysis confirmed the presence of clay minerals in the coarse-particle fraction. Although quartz and feldspars are common in the fine size fractions of Nordic clayey soils, the C/QF ratio indicated that clay minerals on the whole were somewhat more prevalent in several of the leachates relative to standard  $<2 \mu\text{m}$  soil-clay fractions (Table 3), suggesting a preponderance of very fine-clay materials in most leachates. An  $\text{Fe}_2\text{O}_3$  component between 10 and 20 % was also present. Oxalate was able to dissolve  $<10$  % of Al and Fe in the coarse fractions, indicating that most of these elements existed in crystalline phases.

The fine particles, on the other hand, had less  $\text{Al}_2\text{O}_3$  and  $\text{SiO}_2$ , and more CaO, MgO and  $\text{Na}_2\text{O}$ , suggesting the presence of remaining soluble salts in the isolated fractions (Table 2). In two fine fractions (Lilla Böslid and Mellby), the oxalate extraction indicates that most Fe was present in a non-crystalline form (Table 2). The sum of major oxides had a large deficit to 100 % in all fine fractions. However, these freeze-dried powders were highly hygroscopic, and despite the drying procedures it is uncertain to what extent the deficit represents organic constituents or moisture in the samples. Unfortunately, the scarce availability of isolated fractions did not allow an independent measurement of their organic-C content.

Total  $\text{P}_2\text{O}_5$  in both coarse and fine particles was fractions of a percent, generally with somewhat higher concentrations in coarse than in fine particles (Table 2). Total S concentrations are expressed as the oxide  $\text{SO}_3$  in Table 2, although organic forms were dominant as shown below. Its concentration was consistently higher in fine than coarse particles, indicating a higher organic-matter content in the former. The oxalate extractant dissolved 30–73 % of the P in coarse and fine particles and was strongly correlated with total P in both (Fig. S2). For S, the extractability was higher, at approximately 80 % or more (Table 2).

**Table 2**

Bulk oxides (weight percent) of coarse (>0.45  $\mu\text{m}$ ) and fine (<0.45  $\mu\text{m}$ ) particles isolated from leachates collected at the four experimental sites. Extractability by 0.2 M  $\text{NH}_4$  oxalate is the ratio of oxalate-extractable to bulk for each of the elements Al, Si, Fe and P.

Constituent	Kruseberg		Lilla Böslid		Lanna		Mellby	
	>0.45 $\mu\text{m}$	<0.45 $\mu\text{m}$						
<i>Bulk chemistry: Major oxides, weight percent</i>								
Na <sub>2</sub> O	2.2	6.1	5.7	8.6	3.7	17	n.a.	13
MgO	2.8	4.9	4.0	6.0	2.5	7.2	n.a.	3.5
Al <sub>2</sub> O <sub>3</sub>	31	3.2	18	0.05	31	1.8	n.a.	0.35
SiO <sub>2</sub>	36	7.9	23	2.1	36	6.7	n.a.	1.8
P <sub>2</sub> O <sub>5</sub>	0.55	0.23	0.30	0.03	0.40	0.06	n.a.	0.05
SO <sub>3</sub>	0.35	4.2	1.6	3.2	0.34	2.6	n.a.	9.8
K <sub>2</sub> O	8.8	2.7	4.6	0.88	7.3	2.1	n.a.	6.9
CaO	2.1	16	10	21	1.9	12	n.a.	12
MnO	0.06	0.01	0.03	0.0002	0.05	0.002	n.a.	0.002
Fe <sub>2</sub> O <sub>3</sub>	17	1.8	9.3	0.03	14	0.69	n.a.	0.22
Sum	101	47	76	42	96	49	n.a.	48
<i>Extractability by 0.2 M NH<sub>4</sub> oxalate, pH 3: Weight percent of bulk oxide</i>								
Al <sub>2</sub> O <sub>3</sub>	3	4	4	11	4	4	n.a.	56
SiO <sub>2</sub>	1	2	0.5	3	0.5	8	n.a.	n.a.
Fe <sub>2</sub> O <sub>3</sub>	8	13	9	70	10	15	n.a.	77
P <sub>2</sub> O <sub>5</sub>	62	73	55	30	57	48	n.a.	49
SO <sub>3</sub>	87	99	90	79	90	101	n.a.	90

**Table 3**

Distribution of clay minerals (approximate relative weight percent) in leached particles >0.45  $\mu\text{m}$  and the ratio of clay minerals to quartz and feldspars (C/QF-ratio) of (mean over two plots); shown for comparison are ranges of C/QF-ratios observed in the soil profiles of standard <2 $\mu\text{m}$  clay fractions at each site.

Component	Kruseberg	Lilla Böslid	Lanna	Mellby
<i>Clay minerals, weight percent of their sum</i>				
Chlorite	5	0	0	n.a.
Kaolinite	4	0	3	n.a.
Illite	45	29	16	n.a.
Expandable	47	71	82	n.a.
<i>Sum of clay minerals vs sum of quartz and feldspars, weight ratio</i>				
C/QF-ratio, leachates	3.1	0.95	1.2	n.a.
C/QF-ratio, soil	0.8–2.2	0.4–1.5	0.2–0.8	0.4–0.8

### 3.2. Overall P and S speciation

Bulk P K-edge XANES showed that Al-P and org-P were predominant P species in coarse as well as fine particles; Ca-P was also prominent in most isolated materials (Table 4 and Fig. S3). Fe-P, on the other hand, was the least abundant, generally accounting for less than 10 % of the P. Spot-wise  $\mu$ -XANES obtained from the coarse particles (>0.45  $\mu\text{m}$ ), which constituted the majority of leached particles from most sites, shed some more light on this result. Across all the spots and sites, Al-P and Ca-P were more or less ubiquitous at concentration ranges of 20–50 % and 10–30 %, respectively (Figs. 1–3b). Org-P was common, while also showing high variability within several of the samples. Fe-P overall appeared as the least abundant P species in the coarse particles, as it

was detected only in certain areas of the samples from Kruseberg and Lilla Böslid. The samples of fine particles (<0.45  $\mu\text{m}$ ) were generally richer in org-P, and the content of Fe-P reached high levels in certain areas according to the LCF (Figs. 4–6b and c).

Average spot-wise S K-edge  $\mu$ -XANES showed that organic S accounted for 75–97 % of the total S in the coarse particles (Table 5), with the thiol and sulfate ester groups being the predominant portion of organic S (Figs. 1c, 2c and 3c). The proportion of reduced S species was quite variable, with a high percentage in the coarse fraction of Lilla Böslid (Table 5). Similarly to the coarse fraction, organic S species accounted for 89 % of the total S in the fine particles at Kruseberg (Table 5) with thiols and sulfate ester groups being the dominant form of organic S, accounting for 75 % of the total S (Fig. 4c). Similar results were obtained for the other two sites with organic S accounting for 97 and 95 % of the total S in Lanna and Mellby respectively (Table 5). While the reduced thiol groups constituted the main portion (77 %) of organic S in Lanna, a high proportion (27 %) of total S in the particles at Mellby was in the form of sulfonate, a result that is unique to Mellby (Figs. 5c and 6c).

Although high quality XANES spectra and fits were obtained for all samples, there was a slight miss-fit of the S standards to the S K-edge XANES in Mellby, especially at the thiol and sulfoxide XANES region (2471–2477 eV). This may be due to the presence of other thiol and sulfoxide compounds than the L-methionine, L-cysteine, tiosalicylic acid and sodium dimethyl sulfoxide used to model the region. Nevertheless, there are clear indications of the presence of thiol and sulfoxide functional groups in the S K-edge XANES spectra from Mellby.

**Table 4**

Percentage phosphorus speciation in size-fractionated particles from natural leachates water from Swedish agricultural soils as evidenced by linear combination fitting (LCF) of bulk particles P K-edge XANES spectra. Means  $\pm$  standard deviation for the best ten LCF combinations.

P species	Kruseberg		Lilla Böslid		Lanna		Mellby	
	>0.45 $\mu\text{m}$	<0.45 $\mu\text{m}$						
Org-P	21 $\pm$ 3	28 $\pm$ 2	19 $\pm$ 3	n.a.	39 $\pm$ 2	39 $\pm$ 2	n.a.	46 $\pm$ 3
Al-P	39 $\pm$ 13	42 $\pm$ 1	50 $\pm$ 15	n.a.	45 $\pm$ 2	39 $\pm$ 6	n.a.	21 $\pm$ 2
Ca-P	25 $\pm$ 4	32 $\pm$ 2	23 $\pm$ 3	n.a.	16 $\pm$ 2	17 $\pm$ 2	n.a.	3 $\pm$ 3
Fe-P	14 $\pm$ 19	-	9 $\pm$ 16	n.a.	-	4 $\pm$ 6	n.a.	30 $\pm$ 5

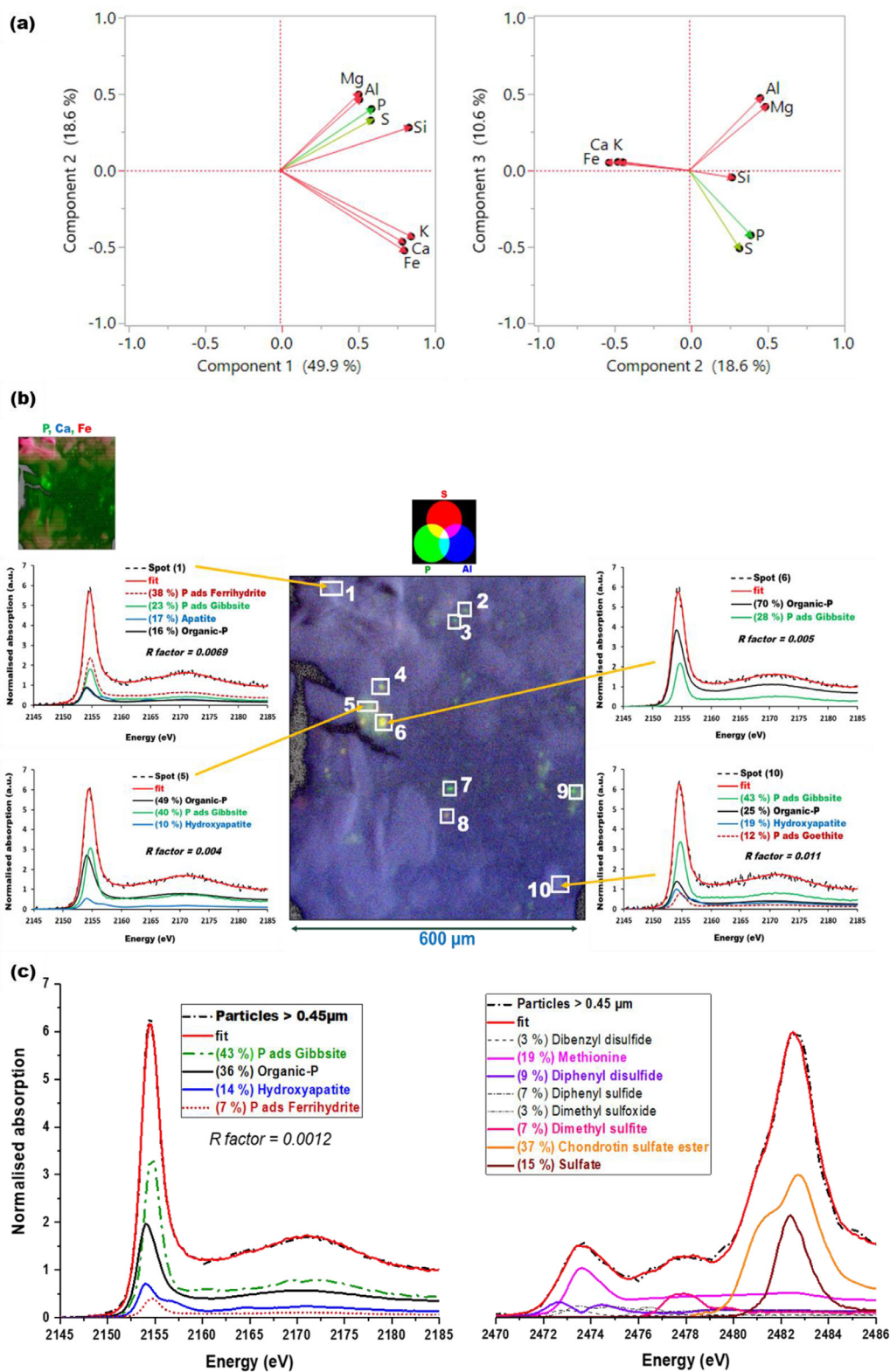


**Fig. 1.** (a) Loadings from principal components analysis of Mg, Si, Al, P, S, K, Ca and Fe, indicating the degree of spatial co-localisation, (b) micro-scale variation in the spatial distribution of phosphorus species and (c) average phosphorus and sulfur speciation in coarse particle (> 0.45 μm) leached from Krusenberg.

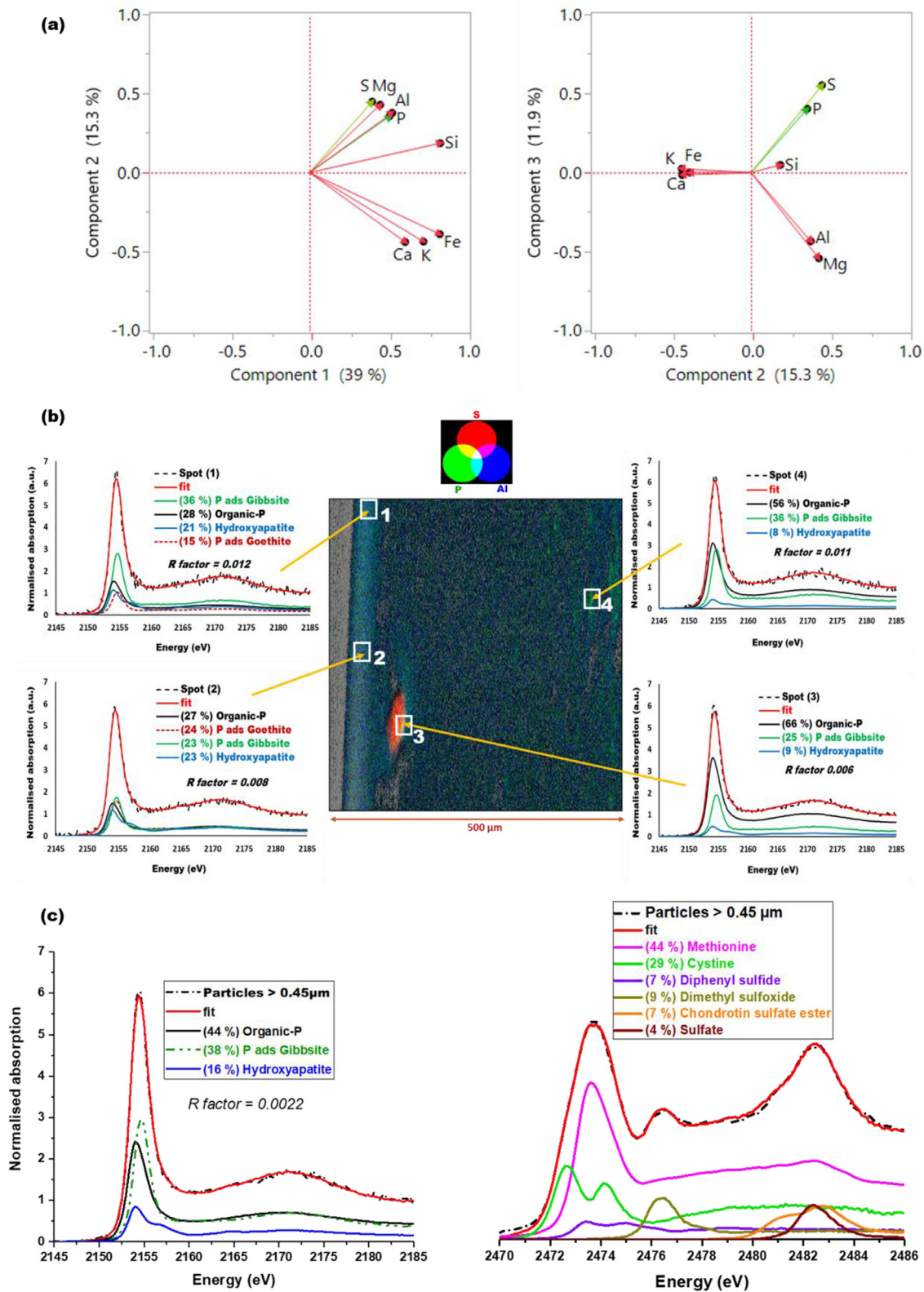
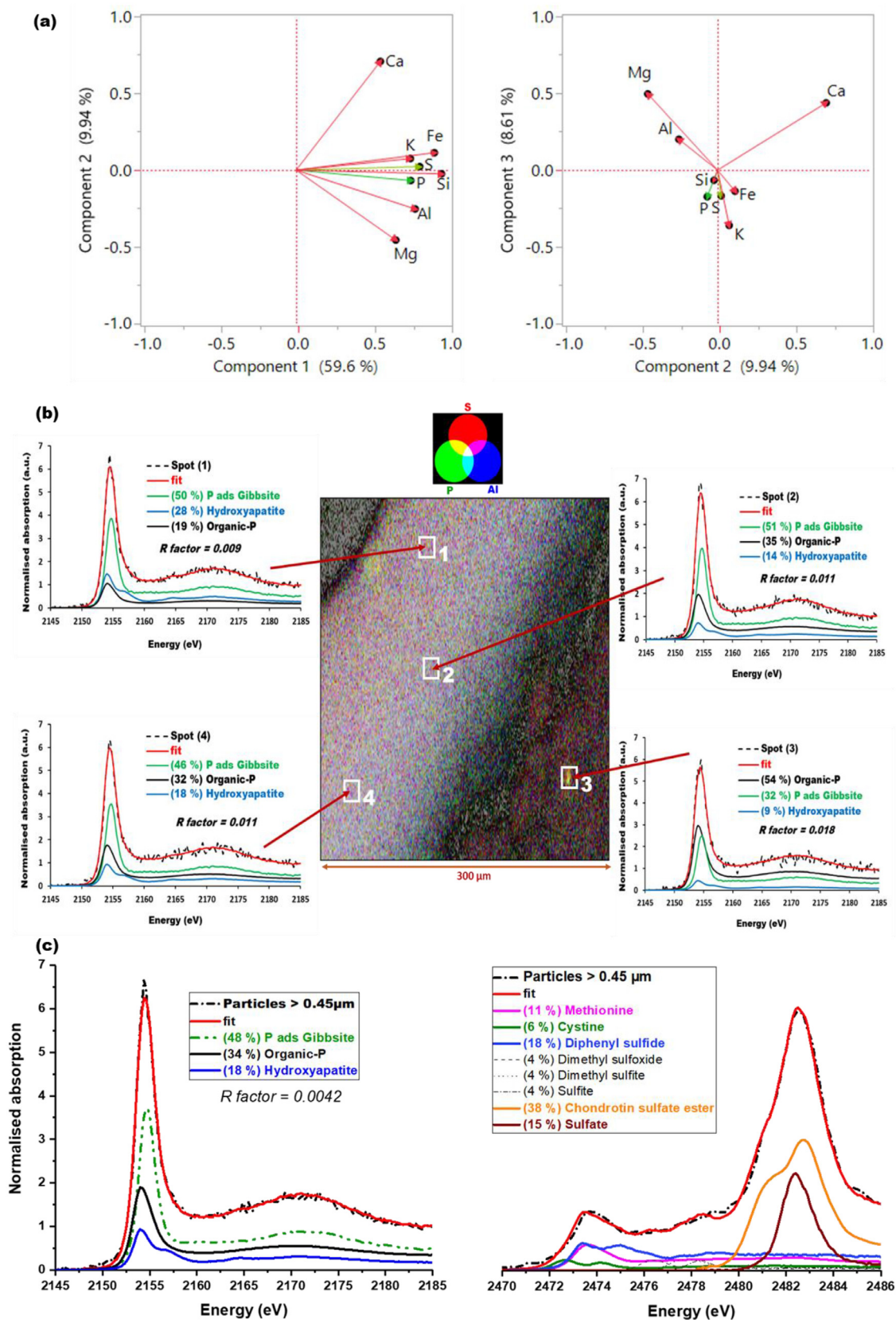


Fig. 2. (a) Loadings from principal components analysis of Mg, Si, Al, P, S, K, Ca and Fe spatial co-localisations, (b) micro-scale variation in the spatial distribution of phosphorus species and (c) average phosphorus and sulfur speciation in coarse particle (> 0.45 μm) leached from Lilla Böslid.



**Fig. 3.** (a) Loadings from principal components analysis of Mg, Si, Al, P, S, K, Ca and Fe spatial co-localisations, (b) micro-scale variation in the spatial distribution of phosphorus species and (c) average phosphorus and sulfur speciation in coarse particle (> 0.45 μm) leached from Lanna.

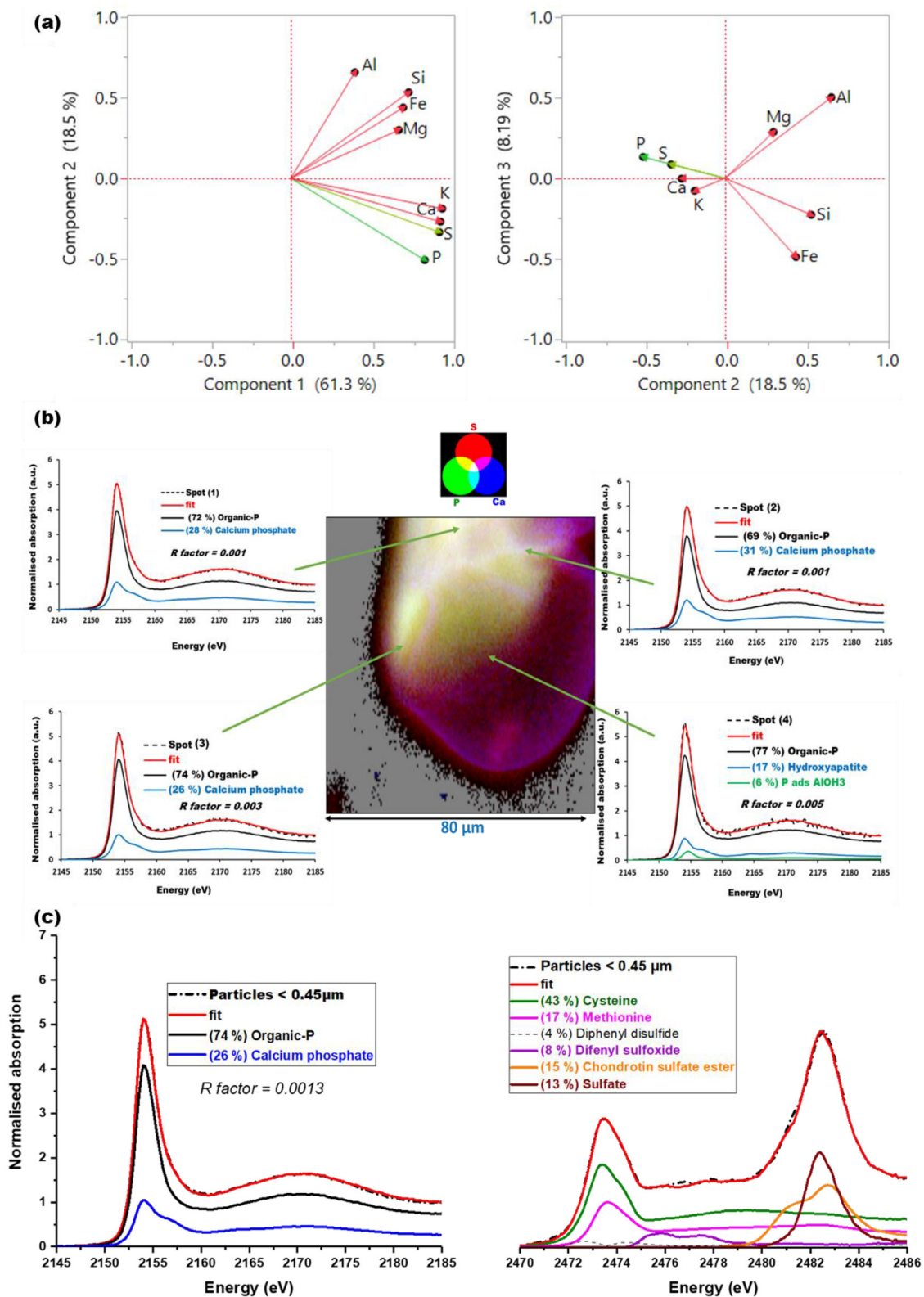
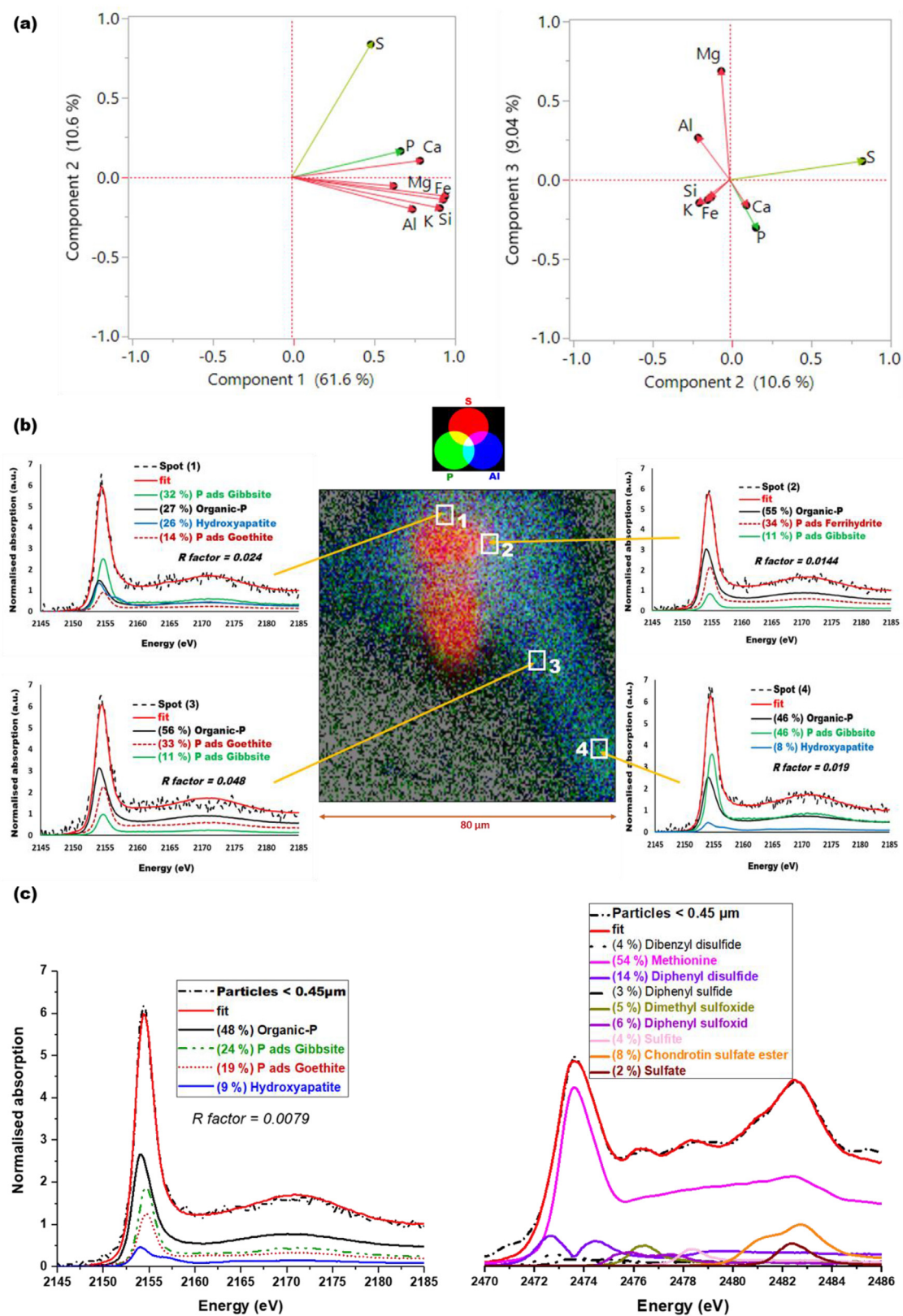
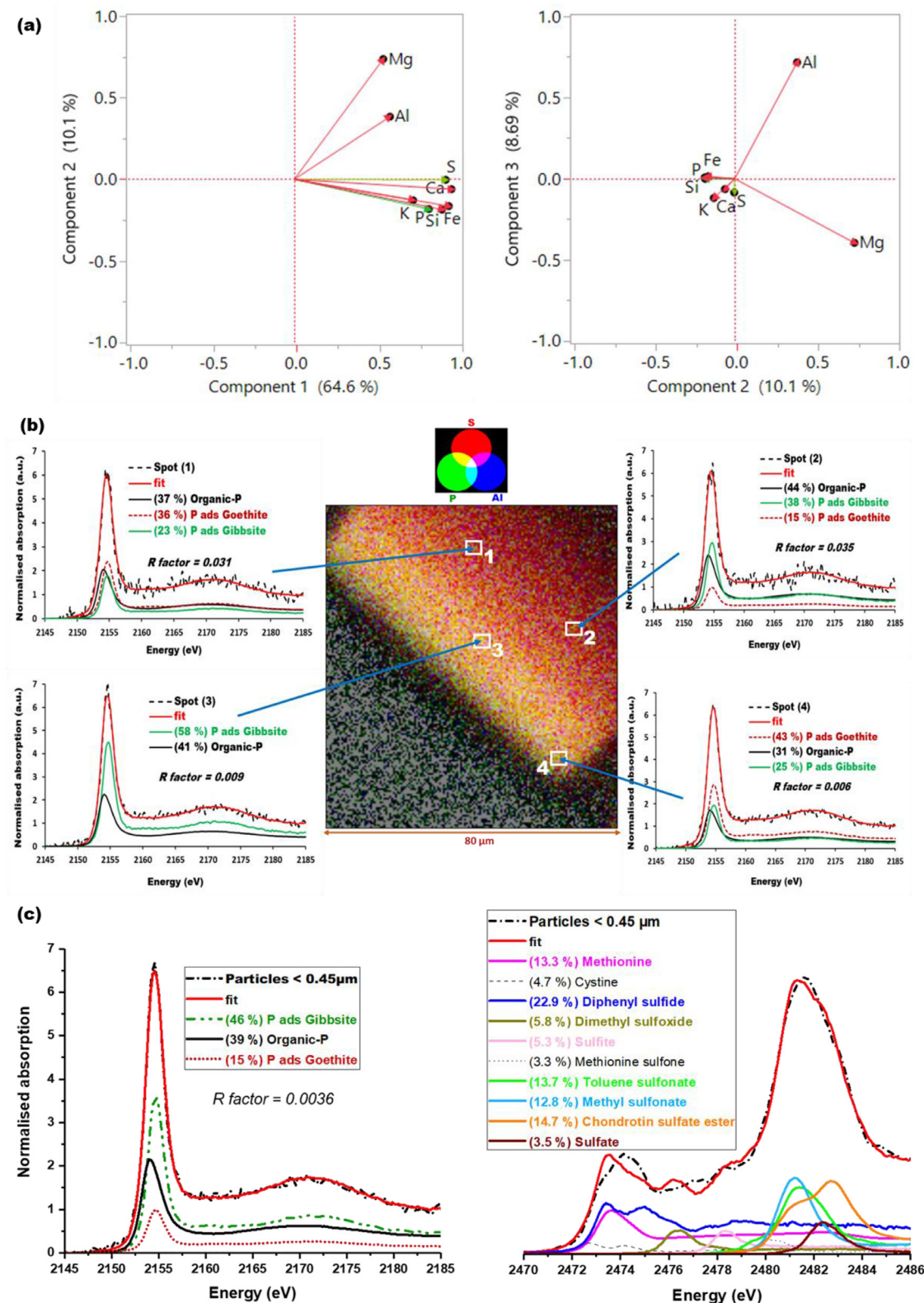


Fig. 4. (a) Loadings from principal components analysis of Mg, Si, Al, P, S, K, Ca and Fe spatial co-localisations, (b) micro-scale variation in the spatial distribution of phosphorus species and (c) average phosphorus and sulfur speciation in fine particle (< 0.45 μm) leached from Krusenberg.



**Fig. 5.** (a) Loadings from principal components analysis of Mg, Si, Al, P, S, K, Ca and Fe spatial co-localisations, (b) micro-scale variation in the spatial distribution of phosphorus species and (c) average phosphorus and sulfur speciation in fine particle (< 0.45 μm) leached from Lanna.



**Fig. 6.** (a) Loadings from principal components analysis of Mg, Si, Al, P, S, K, Ca and Fe spatial co-localisation, (b) micro-scale variation in the spatial distribution of phosphorus species and (c) average phosphorus and sulfur speciation in fine particle (< 0.45 μm) leached from Mellby.

**Table 5**

Percent distribution of sulfur species in sample-average spectra obtained from micro-focused S K-edge XANES (cf. Figs. 1c, 2c and 3c) and as evidenced by LINST fitting using selected model S spectra. 'Reduced S' corresponds to the thiol-S peak; 'intermediately oxidized' is the sum of sulfoxide and/or dimethylsulfite.

S species		Krusenberg		Lilla Böslid		Lanna		Mellby	
		>0.45 $\mu\text{m}$	<0.45 $\mu\text{m}$						
Organic	Reduced	37	63	81	n.a.	35	77	n.a.	41
	Intermediate	15	9	10	n.a.	15	13	n.a.	40
	Sulfate ester	34	17	7	n.a.	36	7	n.a.	15
Inorganic	Sulfate	14	11	3	n.a.	14	3	n.a.	5

### 3.3. Spatial relationships in coarse particles (>0.45 $\mu\text{m}$ )

Of the most abundant elements (Mg, Al, Si, K, Ca and Fe), considerable variability in intensity occurred over distances smaller than the resolution of the beam (1.0  $\mu\text{m}$ ). However, aggregation of particles did occur, with areas of different intensity from the different elements (Figs. S4a, S5a, S6a). PCA was applied on deconvoluted element intensities. Whereas the first principal component (PC1) mainly expressed variations in sample thickness (overall intensity) across the mapped area, the second and higher PCs captured differences in the spatial distribution of different elements. In all coarse samples (Krusenberg, Lanna, Lilla Böslid), the PCA demonstrated spatial correlation between P and S through PC1–PC3 (Figs. 1a, 2a and 3a). Also the RGB correlator identified “hot spots” with co-localization of P and S (yellow in Figs. S4b, S5b, S6b). These spots showed a high proportion of organic P according to  $\mu$ -XANES (Figs. 1–3b), suggesting that P in organic matter was associated with discrete aggregates with a high content also of S. For Fe-P,  $\mu$ -XANES indicated its presence in areas that were high in Fe in the coarse samples from Krusenberg (Figs. 1b and S4) and Lilla Böslid (Figs. 2b and S5). The S, in its turn, ranged from reduced forms (e.g. thiol) to intermediately oxidized (sulfoxide and dimethylsulfite) and highly oxidized (sulfonate and sulfate) groups (Figs. 1c, 2c and 3c). Most importantly, the co-occurrence of org-P with the mainly organic S species strengthened the evidence of P associated with organic matter leaching from the soils.

### 3.4. Spatial relationships in fine particles (<0.45 $\mu\text{m}$ )

Similarly to the coarse fraction, aggregation occurred, with areas of different intensity from the different elements (Figs. S7a, S8a, S9a), and PCA indicated that P was closely related to S (Figs. 4a, 5a and 6a). Spot-wise P K-edge XANES analysis in fine particles leached from Krusenberg (Fig. 4b) and Mellby (Fig. 6b) showed little spatial variation in P speciation. In both samples, org-P was important, constituting up to 74 % of the P at the former site. Organic P was prominent also in the heterogeneous sample from Lanna (Figs. 5b). Spots high in org-P were found at the aggregate to be high also in S (spot 2 in Fig. 5b), as well as in the matrix beside it (spot 3 in Fig. 5b). Similarly to the coarse particles, Fe-P was found sporadically, with high proportions according to LCF in some spots in samples from Lanna and Mellby, while absent at others. Ca-P forms were ubiquitous in the sample from Krusenberg, present in some spots of the Lanna sample, and absent in Mellby.

## 4. Discussion

Leaching of colloidal soil materials involves at least partial dispersion of soil aggregates. The latter consist of various proportions of clay minerals, oxides and organic matter (Totsche et al., 2018), where surface complexes or coprecipitation form intimate associations of organic and mineral materials (Kleber et al., 2015). The stability of these associations may be disrupted by processes affecting either of the solid phases involved. Our combination of bulk-

chemistry quantification, mineralogical analysis, multi-elemental  $\mu$ -XRF imaging, and P and S K-edge XANES on bulk- and spatially-resolved samples, revealed that P speciation was potentially influenced by both phyllosilicate clays, non-crystalline Al- and Fe oxides and organic matter. Although consistent with previous analyses of particles isolated from soils and natural waters (Gottselig et al., 2017b; Jiang et al., 2015; Liu et al., 2014; Missong et al., 2018), our work demonstrates a large diversity in the speciation of P and S at the micron-scale even in leachates from a single site.

Across sites and fractions, the two most common P forms were org-P and Al-P (Table 4, Fig. S12a). Organic P within particulate organic matter in surface waters is composed of diverse molecular forms including glycerol phosphate, guanosine monophosphate, nicotinamide adenine dinucleotide phosphate and inositol hexakisphosphate (Cheesman et al., 2014; Zhang et al., 2019). The presence of organic S species, which ranged from reduced S species like thiols and sulfoxides to fully oxidized sulfate esters and minor amounts of inorganic sulfate (Table 5) and often was co-localized with the P, further supports the leaching of organic P-bearing components, probably derived from soil organic matter in the top soil.

Because phosphate is well known to adsorb to hydrous Fe- and Al oxides (Kingston et al., 1972), it is not surprising that an appreciable amount of particulate P was found to be adsorbed to such surfaces according to the LCF. In Table 6, the P-binding conditions on non-crystalline Al- and Fe-bearing phases in leached particles are explored. Site- and fraction percentages of the average Al-P and Fe-P (Table 4) combined with the total  $\text{P}_2\text{O}_5$  (Table 2) suggest that per kg of leached particles, between 0.67 and 15 mmol P was associated with Al, and up to 5.4 mmol P with Fe. Furthermore, Table 2 suggests that oxalate-extractable Al and Fe represented 0.052–11 g  $\text{Al}_2\text{O}_3$  and 0.20–14 g  $\text{Fe}_2\text{O}_3$  per kg. Table 6 shows that Fe-P relative to oxalate-extractable  $\text{Fe}_2\text{O}_3$  generally represented a ratio not exceeding the sorption capacity of ferrihydrite of approximately 1000 mmol P  $\text{kg}^{-1}$   $\text{Fe}_2\text{O}_3$  (Hesterberg, 2010). In most cases, also Al-P relative to oxalate-extractable  $\text{Al}_2\text{O}_3$  was within the binding capacity of amorphous  $\text{Al}(\text{OH})_3$ , 2500 mmol P  $\text{kg}^{-1}$   $\text{Al}_2\text{O}_3$  (Khare et al., 2005), while apparently exceeding it in one or two of the fine fractions. Phyllosilicates, on the other hand, were dominated by 2:1 minerals and constituted roughly half the mineral mass of leached coarse particles according to C/QF ratios around 2 (Table 3). With 8–13 mmol  $\text{kg}^{-1}$  overall P sorption capacity of 2:1 minerals (Violante and Pigna, 2002), their contribution of P sorption sites could be of the order of 5 mmol  $\text{kg}^{-1}$  in the coarse particles. This is somewhat less than the Al-P and Fe-P of the coarse fraction, although a significant part of it (Table 6). Hence, sorption sites in non-crystalline oxides of Al and Fe in most samples could explain all the Al-P and Fe-P present in the leachates, although phyllosilicates cannot be ruled out as sorbents for part of these species.

Interactions between organic matter, P and Al are not fully deciphered by K-edge XANES. Aluminum ions complex-bound to soil organic matter can, in its turn, adsorb phosphate in a ternary complex (Gerke, 2010; Libeck and Dziejowski, 2008) at P/Al ratios higher than those characteristic of P sorbed at Al hydrous-oxide

**Table 6**

P bound to Al and Fe expressed as mmol of P per kg of leached particles; oxalate-extractable  $\text{Al}_2\text{O}_3$  and  $\text{Fe}_2\text{O}_3$  on the same basis; ratio of (a) over (b).

	Krusenberg		Lilla Böslid		Lanna		Mellby	
	>0.45 $\mu\text{m}$	<0.45 $\mu\text{m}$						
a) P bound to Al and Fe, mmol per kg particles								
Al-P	15	6.7	10	n.a.	13	1.7	n.a.	0.67
Fe-P	5.4	0	1.9	n.a.	0	0.17	n.a.	1.0
a) Oxalate-extractable $\text{Al}_2\text{O}_3$ and $\text{Fe}_2\text{O}_3$ , g per kg particles								
$\text{Al}_2\text{O}_3$	9.1	1.2	6.3	0.052	11	0.6	n.a.	1.9
$\text{Fe}_2\text{O}_3$	14	2.3	8.2	0.20	13	1.0	n.a.	1.7
a) Theoretical P coverage, mmol P per kg oxalate-extractable oxide								
P on $\text{Al}_2\text{O}_3$	1700	5500	1700	n.a.	1200	2700	n.a.	340
P on $\text{Fe}_2\text{O}_3$	380	0	200	n.a.	0	170	n.a.	560

surfaces (Gerke and Hermann, 1992). This is further suggested by hot spots of organic particulate S co-localized with spots with Al-P. Similar observations were made in several studies of particulate P from top forest soils and in stream waters (Gottselig et al., 2014; Gottselig et al., 2017b; Missong et al., 2018). Furthermore, phytate sorbed to an Al hydrous-oxide surface may contribute to the apparent pools of both pure organic P and inorganic P bound to the same mineral surface (Gustafsson et al., 2020); if some of the apparent organic P was associated with Al hydrous-oxide surfaces, the latter might be occupied by P to a larger extent than suggested in Table 6.

The pool of Ca-P is chemically less ambiguous. Although the ability of  $\text{Ca}^{2+}$  to cement organic matter and inorganic minerals and promote the formation of macroaggregates has been well described (Missong et al., 2018; Whittinghill and Hobbie, 2012),  $\text{Ca}^{2+}$  has been reported not to be capable of acting as the metal bridge for the binding of phosphate to organic (e.g. humic) surfaces (Gerke and Hermann, 1992).

On average, less than 10 % of total P was associated to Fe in all particles and across all sites (Table 4). This is in contrast to previous results of P speciation in colloids and nanoparticles isolated by water dispersion from top soils and in surface waters (Gottselig et al., 2017b; Jiang et al., 2015; Liu et al., 2014; Missong et al., 2018), where Fe oxides are known for effective adsorption of phosphate. However, abiotic or bacteria-driven Fe reduction during the oxidation of organic matter is documented as a mechanism of P release in oxygen-depleted environments (Henderson et al., 2012; Murray and Hesterberg, 2006; Warrinnier et al., 2020). Al oxides on the other hand are stable under reducing conditions (Darke and Walbridge, 2000). Additionally, a laboratory study indicated that phosphate released during reductive dissolution of ferrihydrite was re-adsorbed by Al (Murray and Hesterberg, 2006). Overall, the sulfur in the present study was more reduced than in the study of Boye et al. (2011); some samples were comparable to those found under waterlogged conditions by Prieztel et al. (2009a). It may be speculated that fluctuations in redox potential as suspended particles drain through the soil profile kept Fe(III)-bearing colloids as well as P-species associated with ferric-oxide phases at a low level.

Al-P and Fe-P in these soils was largely formed by adsorption of P by non-crystalline minerals of Al and Fe (e.g. allophane and ferrihydrite), which are ubiquitous products of weathering in soils (Eriksson et al., 2016). The high contents of P associated with organic materials and non-crystalline minerals of Al and Fe in the suspended particles of the leachates indicates that studies aiming to characterize these phases, and their associations with the clay minerals that may form the bulk of leached particles, should be prioritized. Organic S and P, and P bound by amorphous Al are highly susceptible to mineralization, which would eventually lead to the release of readily bioavailable nutrients in the receiving wa-

ter bodies. The high abundance of these species in the studied particles makes the mobilization of suspended particles from agricultural land a key driver of eutrophication. Our report of multiple S and P species in the leached particles is therefore of strategic importance in agricultural watershed management, especially in devising technologies to mitigate colloidal driven eutrophication.

## 5. Conclusions

We combined the use of multiple X-ray spectroscopic methodologies to reveal the nature of micro- and nano-sized particles in drain water from four agricultural soils in Sweden. Crystalline mineral phases like illite and expandable phyllosilicates, as well as primary minerals like quartz and feldspars, were major components of the mobilized particles. Nonetheless, non-crystalline (oxalate-extractable) Al and Fe generally could account for P associated with oxide surfaces of these elements according to XANES. However, the somewhat subordinate role of P associated with Fe challenges the common view of Fe as a major carrier for P leaching from the soil, and indicates a need to study the effects of redox reactions in the soil, prior to the leaching, on the export of other P species from the soil profile. Organic P was important in all samples, and associations of P with clusters of organic S indicated the presence of P in micro-aggregates with organic matter. The significance of Al- and Fe-oxides in binding P, indicates a need to intensify research into processes leading to destabilization of their aggregates with phyllosilicate clay and soil organic materials, in order to mitigate eutrophication driven by leaching of particulate macronutrients from agricultural land.

## Declaration of Competing Interest

The authors declare that they have no known competing financial interests or personal relationships that could have appeared to influence the work reported in this paper.

## Acknowledgments

This research was funded by the Swedish Research Council Formas, grant number 2016-01389. We thank the SLRI and ESRF for providing synchrotron beamtime through grant number 2856-1 & 2 and grant number EV-324 respectively. AP thanks Atración de Talento program from Comunidad de Madrid.

## Supplementary materials

Supplementary material associated with this article can be found, in the online version, at doi:10.1016/j.watres.2020.116585.

## References

- Adediran, G.A., Tuyishime, J.M., Vantelon, D., Klysubun, W., Gustafsson, J.P., 2020. Phosphorus in 2D: spatially resolved P speciation in two Swedish forest soils as influenced by apatite weathering and podzolization. *Geoderma* 376, 114550.
- Almkvist, G., Boye, K., Persson, I., 2010. K-edge XANES analysis of sulfur compounds: an investigation of the relative intensities using internal calibration. *J. Synchrotron Radiat.* 17 (5), 683–688.
- Andersson, H., Bergström, L., Djodjic, F., Ulén, B., Kirchmann, H., 2013. Topsoil and subsoil properties influence phosphorus leaching from four agricultural soils. *J. Environ. Qual.* 42 (2), 455–463.
- Bergström, L., Kirchmann, H., Djodjic, F., Kyllmar, K., Ulén, B., Liu, J., Andersson, H., Aronsson, H., Börjesson, G., Kynkäänniemi, P., 2015. Turnover and losses of phosphorus in Swedish agricultural soils: long-term changes, leaching trends, and mitigation measures. *J. Environ. Qual.* 44 (2), 512–523.
- Boye, K., Almkvist, G., Nilsson, S., Eriksen, J., Persson, I., 2011. Quantification of chemical sulphur species in bulk soil and organic sulphur fractions by S K-edge XANES spectroscopy. *Eur. J. Soil Sci.* 62 (6), 874–881.
- Cheesman, A.W., Turner, B.L., Reddy, K.R., 2014. Forms of organic phosphorus in wetland soils. *Biogeochemistry* 11 (23), 6697–6710.
- Church, C., Spargo, J., Fishel, S., 2017. Strong acid extraction methods for “total phosphorus” in soils: EPA method 3050B and EPA Method 3051. *Agric. Environ. Lett.* 2 (1), 1–3.
- Council, N.R., 2011. Achieving Nutrient and Sediment Reduction Goals in the Chesapeake Bay: an Evaluation of Program Strategies and Implementation. National Academies Press.
- Darke, A.K., Walbridge, M.R., 2000. Al and Fe biogeochemistry in a floodplain forest: implications for P retention. *Biogeochemistry* 51 (1), 1–32.
- Das, R., Purakayastha, T., Das, D., Ahmed, N., Kumar, R., Biswas, S., Walia, S., Singh, R., Shukla, V., Yadava, M., 2019. Long-term fertilization and manuring with different organics alter stability of carbon in colloidal organo-mineral fraction in soils of varying clay mineralogy. *Sci. Total Environ.* 684, 682–693.
- Eriksson, A.K., Hillier, S., Hesterberg, D., Klysubun, W., Ulén, B., Gustafsson, J.P., 2016. Evolution of phosphorus speciation with depth in an agricultural soil profile. *Geoderma* 280, 29–37.
- Eriksson, A.K., Ulén, B., Berzina, L., Iital, A., Janssons, V., Sileika, A., Toomsoo, A., 2013. Phosphorus in agricultural soils around the Baltic Sea—comparison of laboratory methods as indices for phosphorus leaching to waters. *Soil Use and Manage* 29, 5–14.
- Fakhræe, M., Li, J., Katsev, S., 2017. Significant role of organic sulfur in supporting sedimentary sulfate reduction in low-sulfate environments. *Geochim. Cosmochim. Acta* 213, 502–516.
- Gerke, J., 2010. Humic (organic matter)-Al (Fe)-phosphate complexes: an underestimated phosphate form in soils and source of plant-available phosphate. *Soil Sci.* 175 (9), 417–425.
- Gerke, J., Hermann, R., 1992. Adsorption of orthophosphate to humic-Fe-complexes and to amorphous Fe-oxide. *J. Plant. Nutr. Soil Sci.* 155 (3), 233–236.
- Gimbert, L.J., Worsfold, P.J., Haygarth, P.M., 2007. Processes affecting transfer of sediment and colloids, with associated phosphorus, from intensively farmed grasslands: colloid and sediment characterization methods. *Hydrol. Process.* 21 (2), 275–279.
- Gottselig, N., Amelung, W., Kirchner, J.W., Bol, R., Eugster, W., Granger, S.J., Hernández-Crespo, C., Herrmann, F., Keizer, J.J., Korkiakoski, M., 2017a. Elemental composition of natural nanoparticles and fine colloids in European forest stream waters and their role as phosphorus carriers. *Glob. Biogeochem. Cycles* 31 (10), 1592–1607.
- Gottselig, N., Bol, R., Nischwitz, V., Vereecken, H., Amelung, W., Klumpp, E., 2014. Distribution of phosphorus-containing fine colloids and nanoparticles in stream water of a forest catchment. *Vadose Zone J.* 13 (7), 1–11.
- Gottselig, N., Nischwitz, V., Meyn, T., Amelung, W., Bol, R., Halle, C., Vereecken, H., Siemens, J., Klumpp, E., 2017b. Phosphorus binding to nanoparticles and colloids in forest stream waters. *Vadose Zone J.* 16 (3), 1–11.
- Gray-Wannell, N., Holliman, P., Greenwell, H., Delbos, E., Hillier, S., 2020. Adsorption of phosphate by halloysite (7Å) nanotubes (HNTs). *Clay Miner.* 55 (2), 184–193.
- Guidry, M.W., Mackenzie, F.T., 2003. Experimental study of igneous and sedimentary apatite dissolution: control of pH, distance from equilibrium, and temperature on dissolution rates. *Geochim. Cosmochim. Acta* 67 (16), 2949–2963.
- Gustafsson, C., Gschwend, P.M., 1997. Aquatic colloids: concepts, definitions, and current challenges. *Limnol. Oceanogr.* 42 (3), 519–528.
- Gustafsson, J.P., Braun, S., Tuyishime, J.R.M., Adediran, G.A., Warrinnier, R., Hesterberg, D., 2020. A probabilistic approach to phosphorus speciation of soils using P K-edge XANES spectroscopy with linear combination fitting. *Soil Syst.* 4 (26).
- Hall, G.E., Bonham-Carter, G., Horowitz, A., Lum, K., Lemieux, C., Quemerais, B., Garbarino, J., 1996. The effect of using different 0.45 μm filter membranes on ‘dissolved’ element concentrations in natural waters. *Appl. Geochem.* 11 (1–2), 243–249.
- Heathwaite, L., Haygarth, P., Matthews, R., Preedy, N., Butler, P., 2005. Evaluating colloidal phosphorus delivery to surface waters from diffuse agricultural sources. *J. Environ. Qual.* 34 (1), 287–298.
- Henderson, R., Kabengi, N., Mantripragada, N., Cabrera, M., Hassan, S., Thompson, A., 2012. Anoxia-induced release of colloid- and nanoparticle-bound phosphorus in grassland soils. *Environ. Sci. Technol.* 46 (21), 11727–11734.
- Hesterberg, D., 2010. Macroscale chemical properties and X-ray absorption spectroscopy of soil phosphorus. In: Singh, B., Gräfe, M. (Eds.), *Developments in Soil Science*. Elsevier, pp. 313–356.
- Hill, D.M., Applin, A.C., 2001. Role of colloids and fine particles in the transport of metals in rivers draining carbonate and silicate terrains. *Limnol. Oceanogr.* 46 (2), 331–344.
- Hillier, S., 2003. Quantitative analysis of clay and other minerals in sandstones by X-ray powder diffraction (XRPD). In: Worden, R.H., Morad, S. (Eds.), *Clay Mineral Cements in Sandstones: International Association of Sedimentologists Special Publication*, 34, pp. 213–251.
- Holtzman, J., Lehman, J.T., 1998. *Environmental Change and Response in East African Lakes*. Kluwer Academic Publishers, Springer, pp. 89–98.
- ISO-6878, 2004. Water quality—determination of phosphorus—ammonium molybdate spectrometric method. ISO 6878: 2004. Int. Org. Stand.
- ISO-15923-1:2013 (2013) Water quality—determination of selected parameters by discrete analysis systems—part 1: ammonium, nitrate, nitrite, chloride, orthophosphate, sulfate and silicate with photometric detection. pp. 12.
- Jarvie, H., Neal, C., Rowland, A., Neal, M., Morris, P., Lead, J., Lawlor, A., Woods, C., Vincent, C., Guyatt, H., 2012. Role of riverine colloids in macronutrient and metal partitioning and transport, along an upland-lowland land-use continuum, under low-flow conditions. *Sci. Total Environ.* 434, 171–185.
- Jiang, X., Bol, R., Nischwitz, V., Siebers, N., Willbold, S., Vereecken, H., Amelung, W., Klumpp, E., 2015. Phosphorus containing water dispersible nanoparticles in arable soil. *J. Environ. Qual.* 44 (6), 1772–1781.
- Khare, N., Hesterberg, D., Martin, J.D., 2005. XANES investigation of phosphate sorption in single and binary systems of iron and aluminum oxide minerals. *Environ. Sci. Technol.* 39 (7), 2152–2160.
- Kingston, F., Posner, A., Quirk, J.T., 1972. Anion adsorption by goethite and gibbsite: I. The role of the proton in determining adsorption envelopes. *J. Soil Sci.* 23 (2), 177–192.
- Kleber, M., Eusterhues, K., Keilweit, M., Mikutta, C., Mikutta, R., Nico, P.S., 2015. Mineral-organic associations: formation, properties, and relevance in soil environments. *Adv. Agron.* 130, 1–140 Vol 130. D. L. Sparks.
- Kleinman, P.J., Fanelli, R.M., Hirsch, R.M., Buda, A.R., Easton, Z.M., Wainger, L.A., Brosch, C., Lowenfish, M., Collick, A.S., Shirmohammadi, A., 2019. Phosphorus and the Chesapeake Bay: lingering issues and emerging concerns for agriculture. *J. Environ. Qual.* 48 (5), 1191–1203.
- Klysubun, W., Tarawarakarn, P., Thamsanong, N., Amonpattaratkit, P., Cholsuk, C., Lapboonrueng, S., Chaichuay, S., Wongtepa, W., 2020. Upgrade of SLRI BL8 beamline for XAFS spectroscopy in a photon energy range of 1–13 keV. *Radiat. Phys. Chem.* 175, 108145.
- Kopriva, S., Malagoli, M., Takahashi, H., 2019. Sulfur nutrition: impacts on plant development, metabolism, and stress responses. *J. Exp. Bot.* 70 (16), 4069–4073.
- Lamers, L.P., Falla, S.J., Samborska, E.M., Dulken, I.A., Hengstum, G.v., Roelofs, J.G., 2002. Factors controlling the extent of eutrophication and toxicity in sulfate-polluted freshwater wetlands. *Limnol. Oceanogr.* 47 (2), 585–593.
- Libeck, B., Dziejowski, J., 2008. Optimization of humic acids coagulation with aluminum and iron (III) salts. *Pol. J. Environ. Stud.* 17 (3), 397–403.
- Liu, J., Hu, Y., Yang, J., Abdi, D., Cade-Menun, B.J., 2015. Investigation of soil legacy phosphorus transformation in long-term agricultural fields using sequential fractionation, P K-edge XANES and solution P NMR spectroscopy. *Environ. Sci. Technol.* 49 (1), 168–176.
- Liu, J., Yang, J., Liang, X., Zhao, Y., Cade-Menun, B.J., Hu, Y., 2014. Molecular speciation of phosphorus present in readily dispersible colloids from agricultural soils. *Soil Sci. Soc. Am. J.* 78 (1), 47–53.
- Ma, X., Li, Y., Li, B., Han, W., Liu, D., Gan, X., 2016. Nitrogen and phosphorus losses by runoff erosion: field data monitored under natural rainfall in Three Gorges Reservoir Area, China. *Catena* 147, 797–808.
- Missong, A., Holzmann, S., Bol, R., Nischwitz, V., Puhmann, H., Wilpert, K.v., Siemens, J., Klumpp, E., 2018. Leaching of natural colloids from forest topsoils and their relevance for phosphorus mobility. *Sci. Total Environ.* 634, 305–315.
- Murray, C.J., Muller-Karulis, B., Carstensen, J., Conley, D.J., Gustafsson, B., Andersen, J.H., 2019. Past, present and future eutrophication status of the Baltic Sea. *Front. Mar. Sci.* 6 (2).
- Murray, G.C., Hesterberg, D., 2006. Iron and phosphate dissolution during abiotic reduction of ferrihydrite-boehmite mixtures. *Soil Sci. Soc. Am. J.* 70 (4), 1318–1327.
- Prentice, M.J., Hamilton, D.P., Willis, A., O’Brien, K.R., Burford, M.A., 2019. Quantifying the role of organic phosphorus mineralisation on phytoplankton communities in a warm-monomictic lake. *Inland Waters* 9 (1), 10–24.
- Prietzl, J., Thieme, J., Tyufekchieva, N., Paterson, D., McNulty, I., Kögel-Knabner, I., 2009a. Sulfur speciation in well-aerated and wetland soils in a forested catchment assessed by sulfur K-edge X-ray absorption near-edge spectroscopy (XANES). *J. Plant. Nutr. Soil Sci.* 172 (3), 393–403.
- Prietzl, J., Tyufekchieva, N., Eusterhues, K., Kögel-Knabner, I., Thieme, J., Paterson, D., McNulty, I., de Jonge, M., Eichert, D., Salomé, M., 2009b. Anoxic versus oxic sample pretreatment: effects on the speciation of sulfur and iron in well-aerated and wetland soils as assessed by X-ray absorption near-edge spectroscopy (XANES). *Geoderma* 153 (3–4), 318–330.
- Prietzl, J., Botzaki, A., Tyufekchieva, N., Brettholle, M., Thieme, J., Klysubun, W., 2011. Sulfur speciation in soil by S K-edge XANES spectroscopy: comparison of spectral deconvolution and linear combination fitting. *Environ. Sci. Technol.* 45 (7), 2878–2886.

- Ravel, B., Newville, M., 2005. ATHENA, ARTEMIS, HEPHAESTUS: data analysis for X-ray absorption spectroscopy using IFEFFIT. *J. Synchrotron Radiat.* 12 (4), 537–541.
- Read, E.K., Ivancic, M., Hanson, P., Cade-Menun, B.J., McMahon, K.D., 2014. Phosphorus speciation in a eutrophic lake by <sup>31</sup>P NMR spectroscopy. *Water Res.* 62, 229–240.
- Regelink, I.C., Koopmans, G.F., van der Salm, C., Weng, L., van Riemsdijk, W.H., 2013. Characterization of colloidal phosphorus species in drainage waters from a clay soil using asymmetric flow field-flow fractionation. *J. Environ. Qual.* 42 (2), 464–473.
- Salomé, M., Cotte, M., Baker, R., Barrett, R., Benseny-Cases, N., Berruyer, G., Bugnazet, D., Castillo-Michel, H., Cornu, C., Fayard, B., 2013. The ID21 scanning X-ray microscope at ESRF. *J. Phys.: Conf. Ser.* 425 (18), 182004.
- SFS-EN13656 (2002) Characterization of waste: microwave assisted digestion with hydrofluoric (HF), nitric (HNO<sub>3</sub>) and hydrochloric (HCl) acid mixture for subsequent determination of elements.
- Sharma, R., Bell, R., Wong, M., 2017. Dissolved reactive phosphorus played a limited role in phosphorus transport via runoff, throughflow and leaching on contrasting cropping soils from southwest Australia. *Sci. Total Environ.* 577, 33–44.
- Sharpley, A., Jarvie, H.P., Buda, A., May, L., Spears, B., Kleinman, P., 2013. Phosphorus legacy: overcoming the effects of past management practices to mitigate future water quality impairment. *J. Environ. Qual.* 42 (5), 1308–1326.
- Sharpley, A.N., Daniel, T., Edwards, D., 1993. Phosphorus movement in the landscape. *J. Prod. Agric.* 6 (4), 492–500.
- Solé, V., Papillon, E., Cotte, M., Walter, P., Susini, J., 2007. A multiplatform code for the analysis of energy-dispersive X-ray fluorescence spectra. *Spectrochim. Acta Part B* 62 (1), 63–68.
- Tannazi, F., Bunker, G., 2005. Determination of chemical speciation by XAFS. *Phys. Scr.* 2005 (T115), 953 2005.
- Totsche, K.U., Amelung, W., Gerzabek, M.H., Guggenberger, G., Klumpp, E., Knief, C., Lehdorff, E., Mikutta, R., Peth, S., Prechtel, A., 2018. Microaggregates in soils. *J. Plant Nutr. Soil Sci.* 181 (1), 104–136.
- Tsao, T.M., Chen, Y.M., Wang, M.K., 2011. Origin, separation and identification of environmental nanoparticles: a review. *J. Environ. Monit.* 13 (5), 1156–1163.
- Ulén, B., Bechmann, M., Fölster, J., Jarvie, H., Tunney, H., 2007. Agriculture as a phosphorus source for eutrophication in the north-west European countries, Norway, Sweden, United Kingdom and Ireland: a review. *Soil Use Manage.* 23, 5–15.
- Ulén, B., Snäll, S., 2007. Forms and retention of phosphorus in an illite-clay soil profile with a history of fertilisation with pig manure and mineral fertilisers. *Geoderma* 137 (3–4), 455–465.
- van Diggelen, J.M., Lamers, L.P., van Dijk, G., Schaafsma, M.J., Roelofs, J.G., Smolders, A.J., 2014. New insights into phosphorus mobilisation from sulphur-rich sediments: time-dependent effects of salinisation. *PLoS ONE* 9 (11), e111106.
- Van Riemsdijk, W., Lyklema, J., 1980. Reaction of phosphate with gibbsite (Al(OH)<sub>3</sub>) beyond the adsorption maximum. *J. Colloid Interface Sci.* 76 (1), 55–66.
- Violante, A., Pigna, M., 2002. Competitive sorption of arsenate and phosphate on different clay minerals and soils. *Soil Sci. Soc. Am. J.* 66 (6), 1788–1796.
- Warrinnier, R., Bossuyt, S., Resseguier, C., Cambier, P., Houot, S., Gustafsson, J.P., Diels, J., Smolders, E., 2020. Anaerobic respiration in the unsaturated zone of agricultural soil mobilizes phosphorus and manganese. *Environ. Sci. Technol.* 54 (8), 4922–4931.
- Werner, F., Prietzel, J., 2015. Standard protocol and quality assessment of soil phosphorus speciation by P K-edge XANES spectroscopy. *Environ. Sci. Technol.* 49 (17), 10521–10528.
- Whittinghill, K.A., Hobbie, S.E., 2012. Effects of pH and calcium on soil organic matter dynamics in Alaskan tundra. *Biogeochemistry* 111 (1–3), 569–581.
- Zhang, C., Feng, W., Chen, H., Zhu, Y., Wu, F., Giesy, J.P., He, Z., Wang, H., Sun, F., 2019. Characterization and sources of dissolved and particulate phosphorus in 10 freshwater lakes with different trophic statuses in China by solution <sup>31</sup>P nuclear magnetic resonance spectroscopy. *Ecol. Res.* 34 (1), 106–118.
- Zou, W., Zhu, G., Cai, Y., Xu, H., Zhu, M., Gong, Z., Zhang, Y., Qin, B., 2020. Quantifying the dependence of cyanobacterial growth to nutrient for the eutrophication management of temperate-subtropical shallow lakes. *Water Res.* 177, 115806.